scientific reports

Check for updates

OPEN

Sting and p53 DNA repair pathways are compromised in Alzheimer's disease

Thomas J. Nelson ✉ & Yunhui Xu

Alzheimer's disease (AD) is the most common cause of dementia. A common finding in AD is DNA damage. Double-strand DNA breaks (DSBs) are particularly hazardous to neurons because their post-mitotic state forces neurons to rely on error-prone and potentially mutagenic mechanisms to repair DNA breaks. However, it remains unclear whether DNA damage results from increased DNA damage or failure of DNA repair. Oligomerization of the tumor suppressor protein p53 is an essential part of DSB repair, and p53 phosphorylated on S15 is an indicator of DNA damage. We report that the monomer:dimer ratio of phosphorylated (S15) p53 is increased by 2.86-fold in temporal lobes of AD patients compared to age-matched controls, indicating that p53 oligomerization is compromised in AD. In vitro oxidation of p53 with 100 nM H_2O_2 produced a similar shift in the monomer:dimer ratio. A COMET test showed a higher level of DNA degradation in AD consistent with double-strand DNA damage or inhibition of repair. Protein carbonylation was also elevated (190% of control), indicating elevated oxidative stress in AD patients. Levels of the DNA repair support protein 14-3-3σ, γ-H2AX, a phosphorylated histone marking double strand DNA breaks, and phosphorylated ataxia telangiectasia mutated (ATM) protein were all increased. cGAS-STING-interferon signaling was impaired in AD and was accompanied by a depletion of STING protein from Golgi and a failure to elevate interferon despite the presence of DSBs. The results suggest that oxidation of p53 by ROS could inhibit the DDR and decrease its ability to orchestrate DSB repair by altering the oligomerization state of p53. The failure of immune-stimulated DNA repair may contribute to cell loss in AD and suggests new therapeutic targets for AD.

The four most important predictive factors for AD are obesity, cardiovascular disease, age, and ApoE4 genotype[1]. What these four factors have in common is the ability to induce or promote DNA damage, which results in chronic inflammation, cell loss, and cellular senescence. DNA damage has long been known to be prominent in AD[2–10] and can lead to failed cell cycle re-entry, cellular senescence, or p53-mediated apoptosis[11]. Widespread somatic gene recombination, possibly initiated by double strand breaks (DSBs), has also been observed in AD, including intra-exonic junctions, insertions, and deletions[9]. There are also reports that ApoE4 interacts in a manner not yet fully understood through thioredoxin[12] and redox-factor 1 to inhibit activation of tumor suppressor protein p53. Upon activation, p53 tetramerizes and binds to DNA, where it participates in DNA repair. Phosphorylation at S15 occurs after DNA damage and leads to decreased interaction with its negative regulator, MDM2[13], which targets p53 for ubiquitination and proteasomal degradation.

Oxidative DNA damage accumulates with age[14], and DSBs are a potential driver for aging[15–17]. DSBs are particularly hazardous to neurons because their post-mitotic state forces neurons to rely on the error-prone and potentially mutagenic mechanism of non-homologous end-joining (NHEJ) instead of error-free homologous recombination (HR) to repair DNA breaks[18,19]. Oxidative stress, which is an important cause of DNA damage, is a key mediator of neuroinflammation[20–22] and cardiovascular disease[23]. Viruses also induce ROS and cytokine release by acting on pattern recognition receptors (PRRs). A high-fat diet creates DSBs via inflammatory cytokines which interfere with DSB rejoining[24,25]. Thus, DNA damage can occur from several seemingly unrelated pathways that are implicated as risk factors for AD.

There is strong evidence that p53 is involved AD pathogenesis[26–31]. p53 is a key component of DSB repair. It has strong effects on both the innate and adaptive immune systems[32] and participates in the inflammatory response to DSBs. In its tetramer form p53 binds DNA, while monomers and loss-of-function mutations, as occur in cancer, contribute to cell proliferation. Activation of p53 in the CNS can induce tau aggregation

Department of Neurology, Marshall University Joan C. Edwards School of Medicine, Huntington, WV 25704, USA. ✉email: nelsonth@marshall.edu

and neurofibrillary tangles[33] and loss of dendritic spines[34]. Conformationally altered p53 in lymphocytes, aka unfolded/aggregated p53, has been proposed as a peripheral marker of early AD[35–43]; however, unfolded p53 has not yet been found in brain. p53 is also activated in obesity[44,45] due to oxidative DNA damage[46–48].

Foreign or fragmented double-strand DNA (dsDNA) in the cytosol caused by viral infections or DNA damage is recognized by the DNA sensor DNA-PKcs (DNA-dependent protein kinase catalytic subunit), which phosphorylates and activates the enzyme cGAS (cyclic GMP-AMP [cGAMP] synthase)[49] to produce the cyclic dinucleotide 2′,3′-cGAMP. cGAMP induces dimerization and activation of STING (Stimulator of Interferon Gene), which translocates from the endoplasmic reticulum to the Golgi and binds to the kinases TBK1 (TANK-binding kinase 1 and IKKβ (IkappaB kinase-β). These kinases activate IRF3 (interferon regulatory factor 3) and NF-κB (nuclear factor kappa-light-chain-enhancer of activated B cells) to induce the expression of interferon-stimulated genes. STING can also stimulate autophagy, necroptosis, and possibly ferroptosis[50] and can induce cellular senescence[51–53], all of which are implicated in AD[54].

In this study we found that p53 oligomerization is inhibited in AD. Monomerization is induced by oxidants such as H_2O_2. The cGAS-STING interferon response in AD is also inhibited due to depletion of STING from Golgi despite high levels of fragmented DNA. The evidence is consistent with impairment of p53 oligomerization from chronic oxidative DNA damage and compromise of the Type I interferon response in AD by interference with TBK1 phosphorylation of IRF3, as occurs in cancer cells.

Materials and methods

Human autopsy samples. Frozen anonymized samples of temporal lobe (Brodmann's Area 38) obtained from AD and unaffected patients at autopsy were acquired from NeuroBioBank through the Human Brain and Spinal Fluid Resource Center, VA W Los Angeles Healthcare Center, Los Angeles, CA. Average age was not significantly different (AD = 77.2 ± 1.85, Control = 76.3 ± 1.9, $\bar{x}$ ± SEM, p = 0.74). Postmortem intervals were also not significantly different between AD and unaffected patients (AD = 14.33 ± 0.73 h, Control = 15.05 ± 0.98 h, n = 20, p = 0.56; n = 20, $\bar{x}$ ± SEM). Both AD and unaffected aged patients had a comparable incidence of hypertension (6/20, 30%), and 50% of patients diagnosed with AD (10/20) also had atherosclerosis or cardiovascular disease compared with 35% (7/20) of controls ($X^2(1, n = 20) = 0.41$, p = 0.52). All experiments were performed in accordance with all relevant guidelines and regulations. In previous experiments, 40% of AD patients but no controls had at least one allele of ApoE4, a known risk factor for AD, obesity, and metabolic syndrome[55] (p = 0.003).

Comet assay. Nuclei from human autopsy temporal lobe samples from AD and age-matched controls were isolated by standard methods. Briefly, 10–20 mg tissue was gently homogenized at 4 °C in 9 volumes of NILR (Nuclear Isolation Lysis Reagent = 10 mM Tris–HCl pH 7.5, 10 mM NaCl, 3 mM $MgCl_2$, 0.1% NP40, 0.25 M sucrose) in the presence of 1 × HALT protease/phosphatase inhibitors (ThermoFisher 78443) in a motorized Teflon homogenizer at 200 rpm. The homogenate was centrifuged at 4 °C and 300*g* for 10 min and the pellet containing enriched nuclei was suspended in 100 µl PBS + 1 × HALT protease/phosphatase inhibitors. Nuclei were counted in a hemacytometer and diluted to 1×10^5 nuclei/ml. Approximately 500–1000 nuclei were added to 45 µl low-melting agarose, plated on Comet slides (Trevigen 4250-050-K), and incubated with lysis solution and alkaline unwinding solution according to the manufacturer's protocol. DNA was electrophoresed at 21 V and 300 mA for 1 h at 4 °C. After staining with SYBR Gold, slides were illuminated with a 100-mW 402 nm semiconductor laser and imaged at 12 bits/channel with a camera and macro lens behind a 530/43 nm FITC emission filter (Thorlabs) from a fixed distance (40 cm) for 5 s. Images were converted to 16-bit grayscale and tail moment, fraction of DNA in the tail[56], and tail length were measured in Imal 3.8.8 software. At least 50 nuclei comet tails from each of the ten samples were selected at random for each measurement.

Dot blots. Tissue samples were homogenized in a Teflon homogenizer at 200 rpm at 1:50 dilution (0.01 g wet weight/0.5 ml) of 10 mM Tris–HCl pH 7.4 containing 1 × HALT protease/phosphatase inhibitors. Homogenates were centrifuged at 15,000*g* in 1.5 ml polypropylene centrifuge tubes for 10 min, transferred to new tubes, and re-centrifuged. Supernatants were injected onto a 4 × 150 mm Inertsil WP300 diol size-exclusion (SEC) HPLC column equilibrated with 0.1 M sodium sulfate + 0.1 M sodium phosphate adjusted to pH 6.65 with phosphoric acid. The flow rate was 0.2 ml/min. The column was calibrated using cytochrome c, hemoglobin, trypsin inhibitor, bovine serum albumin monomer and dimer, ATP, and thyroglobulin. The flow was converted to microdroplets by passing through a 32-gauge hypodermic needle and fractions (0.1 min) were collected by a fraction collector in 1.5-ml polypropylene centrifuge tubes. Fractions were spotted on a reinforced nitrocellulose membrane (Amersham Protran 0.45 µm) in a 96-well suction dot-blot apparatus. The membrane was blocked with BSA and immunostained with p53 phospho-Ser15-specific antibody (Abcam 223868) followed by HRP-linked secondary antibody and imaging of chemiluminescence as described below.

Western blots. Protein concentration in samples was measured in triplicate by mixing 0.03 ml homogenate with 0.1 ml water + 0.1 ml Coomassie Plus Bradford reagent (ThermoFisher 23238). Bovine serum albumin was used as a standard. Absorbance at 595 nm was measured in a Biotek/Agilent Synergy H1 microplate reader. Samples containing 10–30 µg protein were mixed with 0.5 volume of 5 × non-reducing Laemmli buffer, incubated for 3 min at 95°, and applied to a Novex 4–20% polyacrylamide gradient Tris–glycine wedge gel (Fisher XP04202). In some experiments, a 10% gel poured manually in Mini-Protean short plates (BioRad, 1653308) was used instead. Proteins were electrophoretically transferred to nitrocellulose membranes, blocked for 1 h with 2.5% BSA + 10 mM Tris–HCl pH 8.0 + 150 mM NaCl, incubated in TBST for 1–2 h at RT with primary antibody, and washed 3 times with 1xTBST. Blots were incubated 1 h at RT in TBST with HRP-labeled secondary antibody (0.06 µg), then washed with TBST 6× for 3 min. SuperSignal Atto West chemiluminescence substrate (Ther-

moFisher, 38555, 1 ml) was added and membranes were imaged at 16 bits in a custom CCD imaging system. In some experiments, Amersham ECL Prime Western Blotting Detection Reagent (RPN2232) was used instead. To confirm equal loading, membranes were stripped by immersion in RestorePlus Western Blot Stripping Buffer (ThermoFisher 46430), blocked with BSA, and stained for actin, GAPDH, or histone H3. Novex LC5800 colored MW markers (ThermoFisher) were used to calibrate the images.

Antibodies used: phospho-S396 IRF3 = Thermo 720012; pan IRF3 = Thermo 582178; STING = Abcam ab239074; phospho-S366 STING = Cell Signaling 197815; 14-3-3σ = Proteintech 10622010ap; pan p53 = Abcam ab26; phospho-S15 p53 = Abcam ab223868; CEBPβ = Santa Cruz sc-7692; γH2AX = Thermo MA533062; GM130 = R&D Systems mab81991-100; actin = ThermoFisher MA515739; GAPDH = ThermoFisher 585074; histone H3 = Abcam ab176842; ATM = Abcam ab32420; pATM = Abcam ab81292; ATR = Abcam ab2905; pATR = Abcam ab223258.

ELISA kits used: IFNα = PBL Assay 41115-1; IFNβ = PBL Assay 41415-1; Protein carbonylation = Abcam ab238536; phospho T1989/total ATR = Abcam ab279742; phospho S1981/total ATM = Abcam ab279740. Ratios obtained from phospho-ELISA kits were corrected for the different signal responses from the pan- and phospho-specific antibodies used by the kit using phosphoprotein standards. To confirm the ELISA results, all ELISA experiments except for interferon measurements were repeated using Western blots. Protein carbonylation was also confirmed by a Protein Carbonyl Assay Kit (Abcam ab178020) in which the proteins are derivatized with dinitrophenylhydrazine, separated by SDS–polyacrylamide gel electrophoresis, and stained with a DNP-specific antibody according to the manufacturer's instructions.

Protein carbonylation. Protein carbonylation was measured using the colorimetric Abcam Protein Carbonyl Elisa kit (Abcam ab238536) according to the manufacturer's instructions. Frozen samples of the temporal lobe obtained from AD and unaffected patients were prepared by homogenization of tissue in 1xPBS containing 1 × HALT protease/phosphatase inhibitors. Samples (0.25 µg protein) were applied to the ELISA plate. Carbonylation Western blots were performed using a Protein Carbonyl Assay Western Blot kit (Abcam ab178020) according to the manufacturer's instructions. Briefly, 300 µg (around 30 µl) of homogenate was solubilized by combining 30 µl of 2× extraction buffer containing 50 mM dithiothreitol. After a 20 min incubation on ice for 20 min, samples were centrifuged at 18,000×*g* for 20 min at 4 °C. Protein concentration was measured again and aliquots (10 µl) of the solubilized supernatants were denatured with 10 µl of 12% sodium dodecyl sulfate (SDS) for a final concentration of 6% SDS. Samples were derivatized by adding 20 µl of 1× dinitrophenylhydrazine solution and incubated at room temperature for 15 min. Neutralization solution (20 µl) was added and the neutralized samples were applied to a precast 4–20% polyacrylamide gel. Proteins were electrophoretically transferred to nitrocellulose membranes, blocked with bovine serum albumin, and stained using an antibody specific for the DNP moiety in proteins. After 3 × washing with TBST, the membranes were incubated 1 h with LiCor 800CW IRDye anti-rabbit secondary antibody (926-32211) at 1:1000 dilution, washed, and imaged in a custom near-infrared imaging system (excitation = 720–775 nm, emission = 790–810 nm) for 300 s and imaged again for 0.5 s under white light for the MW markers. Images were analyzed densitometrically by scanning horizontally across the image between 30 and 260 kDa.

Imager and software settings. Chemiluminescent Western blots were imaged at 16 bits/pixel in a custom CCD imaging system with an f/1.2 lens using exposures between 7 and 120 s. Densitometry was done using custom image analysis software (Imal 3.8.5). Background subtraction in dot blots was done by partitioning the original 16 bit grayscale values into foreground and background using the fuzzy k-means algorithm in Imal using sampling of the 40 pixel diameter circular region around the spot. This procedure corrected for any minor variations in background across the blot and was validated against other software before use. For Western blots, a 16 bit/channel image was taken with a red, green, and blue filter showing the colored molecular weight markers on the same blot illuminated by a white LED. The 48-bit RGB color image of MW markers was reduced to 24 bits for publication. The chemiluminescence image was color-inverted, converted to 24 bit grayscale, then to 24 bit RGB, and combined with the MW marker image for publication.

Statistical analysis. Statistical tests, including two-variable equal variance Student T tests, error propagation, mean and SEM of chromatograms, and Marquardt–Levenberg nonlinear curve fitting, were done in xdata 1.0.0. Experiments in which two or more factors are measured were analyzed by ANOVA followed by Tukey HSD [Honestly Significant Difference] multiple comparisons of means (95% family-wise confidence level) using R. Other statistics, including power analysis, were calculated in R. Data are shown as mean ± standard error of the mean (SEM) unless otherwise indicated.

Subcellular fractionation. Golgi were isolated using the Invent Biotechnologies Golgi Enrichment Kit (GO-037). This kit was found to produce highly enriched cis-Golgi apparatus and trans-Golgi secretory vesicles as determined by Western blot for Golgi marker GM-130. Tissue was homogenized by grinding 20–50 mg of tissue against the membrane of a filter cartridge with a plastic rod, followed by several centrifugation steps prescribed by the manufacturer. GM-130 is normally dimerized[57] and 100 mM DTT is necessary to observe the monomeric band. Nuclei for Western blot experiments were isolated as described above for Comet analysis except that the NILR extraction step was done twice and the nuclei were sonicated in a Qsonica Q125 125-Watt sonicator for 20 s at 4° and 20% amplitude after isolation.

Results

AD brains exhibit oxidative dsDNA damage but not single-strand DNA (ssDNA) damage. We measured DNA integrity in nuclei isolated from temporal lobe autopsy samples from 5 AD and 5 unaffected patients using the COMET test. This test allows visualization of DNA damage by subjecting nuclei immobilized in agarose to a low-voltage electric field. The amount of DNA degradation is proportional to the tail moment and length of the 'comet' tail. Figure 1 shows that nuclei isolated from AD patients had significantly longer tails than age-matched controls (tail length as tail DNA/total DNA: AD = 0.832 ± 0.018; age-matched control = 0.748 ± 0.017, n = 5, p = 0.0091). Tail moment was also significantly increased (AD = 40.92 ± 3.80; age-matched control = 25.24 ± 0.69, n = 5, p = 0.0034), indicating a higher level of degradation consistent with dsDNA damage or inhibition of DNA repair in AD.

In human AD patients, protein carbonylation, measured by ELISA in samples of temporal lobe (Brodmann's area 38) obtained at autopsy, was 190 ± 26% that of age-matched unaffected controls (Fig. 2a) (N = 20, $p = 2.5 \times 10^{-5}$), indicating elevated oxidative stress in AD. The protein carbonylation changes were confirmed using the DNPH Western blot method (Fig. S01l). Densitometric scans confirmed increased carbonylation in a number of proteins between 30 and 260 kDa (Fig. S01m). Calibration of the Western blot image showed prominent bands at 50, 68, 104, and 155 kDa. This blot also confirms that the oxidized product is proteins and not DNA. However, oxidation of DNA in addition to protein oxidation is not ruled out. Protein carbonylation is an accepted marker of oxidative stress[58–62]. Protein carbonylation in peripheral tissue is observed in obese humans[63] and in mice fed an obesity-inducing diet[64], as well as in human aging[65,66].

DNA damage could be caused by increased oxidative DSBs or by an impairment of the DNA damage response (DDR). To determine whether the DDR is impaired in AD, we used ELISA to measure ataxia telangiectasia mutated (ATM) phosphorylation (S1981), an index of dsDNA repair through the p53 pathway. Pan ATM showed a modest decrease to 87 ± 0.32% of control, while the ratio of pATM/pan ATM was increased to 128 ± 7.8% of control (N = 10, p = 0.00045) (Fig. 2b,c), indicating activation. ATM phosphorylation plays a key role in DDR-induced cell death[11]. Due to possible dephosphorylation in the post-mortem interval, the actual changes in ATM phosphorylation could be larger than observed.

We also measured C/EBPβ, 14-3-3σ, p53-pS15, and γ-H2AX by Western blotting and ATR and phospho-ATR (T1989) by ELISA. The transcription factor C/EBPβ, a marker of neuronal activity-induced cellular growth, was

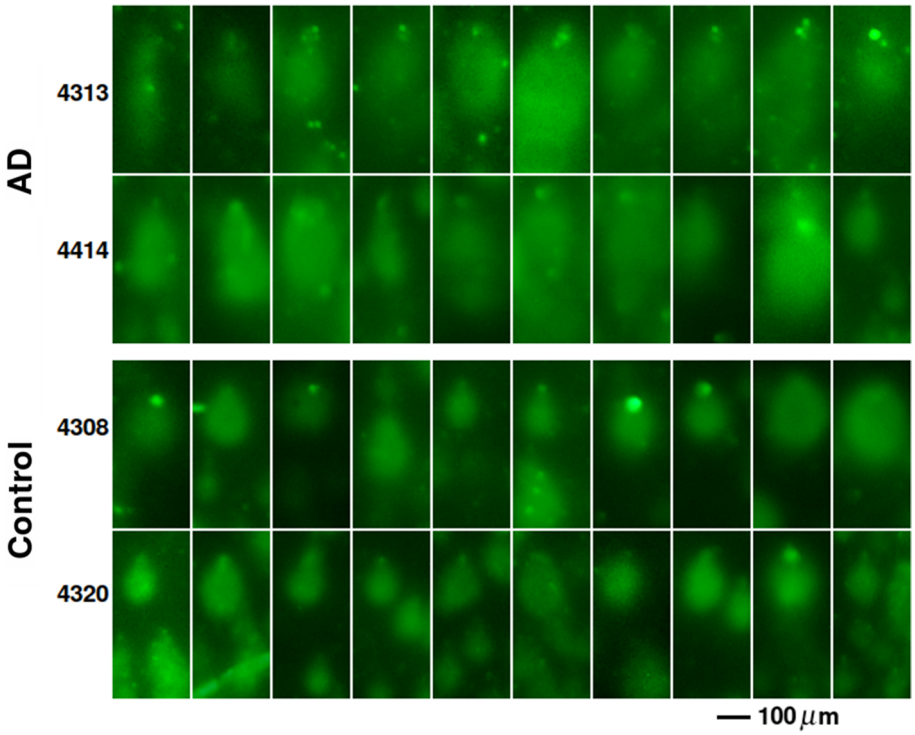

Figure 1. DNA damage is increased in AD. Each panel shows ten randomly selected nuclei isolated from human temporal lobes from two AD and two age-matched control patients. Isolated nuclei were plated onto agarose slides, lysed, and incubated in high-pH unwinding solution. After agarose electrophoresis (4°, 21 V, 1 h), they were stained with SYBR Gold, illuminated with a 402-nm laser, and emission at 530 nm was photographed at a fixed distance from the slide. Representative images are shown. Fifty comets from each image (5 AD and 5 control) were analyzed. Analysis of all ten samples showed that AD samples contained consistently higher percentage of DNA in the tail and increased tail moment (Fraction of DNA in tail: AD = 0.83 ± 0.02; Control = 0.75 ± 0.02, n = 5, p = 0.0091. Tail moment: AD = 1.62 ± 0.16 of control, n = 5, p = 0.0034, two tailed Student's t test), indicating greater dsDNA breakage in the AD samples.

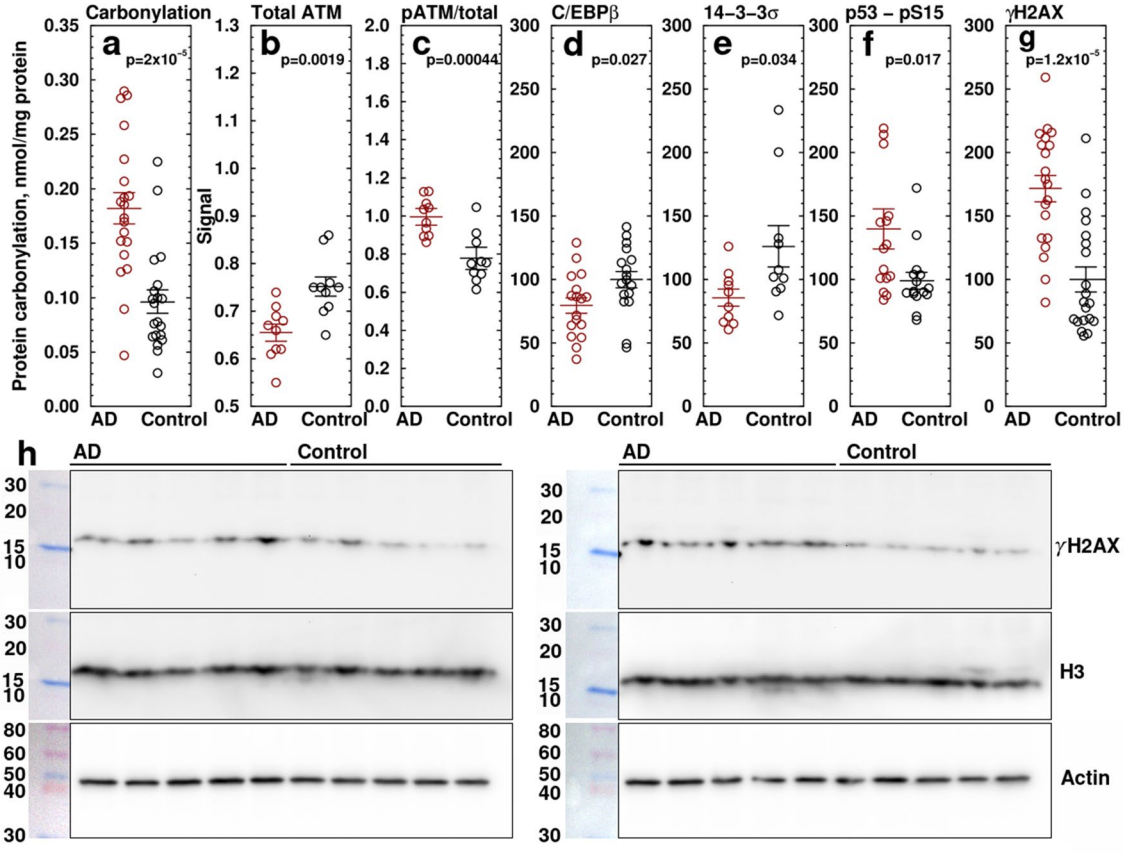

Figure 2. Changes in DNA damage repair-related proteins in brains of AD patients. (**a**) Protein carbonylation measured by ELISA. AD is 1.90 ± 0.26 × control. N = 20, $p = 2.5 \times 10^{-5}$. Protein carbonylation was confirmed using the 2,4-dinitrophenylhydrazine Western blot method (Fig. S01l,m). (**b**,**c**) Phospho- and total (pan-) ATM measured by ELISA. (**b**) Total ATM, AD = 0.655 ± 0.0017, Con = 0.752 ± 0.002, p = 0.0019. (**c**) Ratio of phospho-S1981-ATM/pan-ATM. AD = 0.996 ± 0.044, Con = 0.776 ± 0.058, p = 0.00045. (**d**–**h**) DNA repair markers measured by Western blot. (**d**) C/EBPβ normalized to control, AD = 79.53 ± 6.01, Control = 100 ± 6.40, N = 17, p = 0.027. (**e**) 14-3-3σ, AD = 85.6 ± 6.6, Con = 126.1 ± 16. N = 10, p = 0.034. (**f**) phospho-S15 p53 normalized to control, AD = 135.0 ± 12.0, Control = 100 ± 6.6. N = 15, p = 0.017. (**g**) γH2AX, a marker of DSBs, normalized to control, AD = 171.6 ± 10.3, Control = 100 ± 9.76. N = 20, $p = 1.2 \times 10^{-5}$. (**h**) Representative Western blot of γH2AX in AD and control samples. The combined γH2AX results are shown in the scatterplot (**f**). Western blots were run and developed in parallel under identical conditions. After imaging, blots were stripped and re-stained with histone H3 and actin. Images shown have been cropped for clarity of presentation. Original full-size blots and confirmatory Western blots of the ELISA results are presented in Supplementary Fig. S01a–s. Samples are temporal lobe, Brodmann's area 38. Ages: AD = 77.2 ± 1.9 yr, Control = 76.3 ± 1.9 yr. PMI: AD = 14.33 ± 0.73 h, Control = 15.05 ± 0.98 h, N = 20, p = 0.56 ($\bar{x} \pm$ SEM).

decreased in AD to 79.5 ± 6.0% of control (N = 17, p = 0.027; Figs. 2d, S01a–k). The 14-3-3σ protein stabilizes the p53 tetramer state by preventing mouse double minute 2 homolog (MDM2) binding[67], thereby promoting DNA binding[68]. 14-3-3σ was decreased to 67.9 ± 10% of control (Fig. 2e). p53 phosphorylated on S15, an indicator of DNA damage[69], was elevated to 135 ± 15% in AD samples (AD = 135.0 ± 12.0, Control = 100 ± 6.6, N = 15, p = 0.017 (Fig. 2f). γ-H2AX, a phosphorylated histone marking double strand DNA breaks[70], despite considerable variability, was 1.72 ± 0.20× of controls (Fig. 2g,h; AD normalized to controls = 171.6 ± 10.3, control = 100 ± 9.8, n = 20, $p = 1.2 \times 10^{-5}$). These findings indicate that dsDNA damage is increased in AD. No significant change was observed in ataxia-telangiectasia and Rad3-related protein (ATR), a marker for repair of ssDNA breakage (Fig. 3a), or in its phosphorylation state (Fig. 3b,c) indicating that increased DSBs and dsDNA repair but not ssDNA repair is detectable in AD. The ELISA results for pATM and pATR were confirmed by Western blotting (Figs. S01n,o, S02). Because γ-H2AX is partially localized to nuclei, both histone H3 and actin were used as loading controls (Figs. 2h, S01k).

p53 oligomerization is compromised in AD. Although changes in p53, including unfolding and aggregation in lymphocytes, have been found to occur in AD, measurements of total p53 show modest and sometimes conflicting results, likely due to rapid proteasomal degradation. Changes in p53 oligomerization state in AD have not been reported. We homogenized temporal lobe autopsy samples from AD and age-matched unaffected patients at high dilution (1:50) to avoid artifactual aggregation and measured the oligomerization state

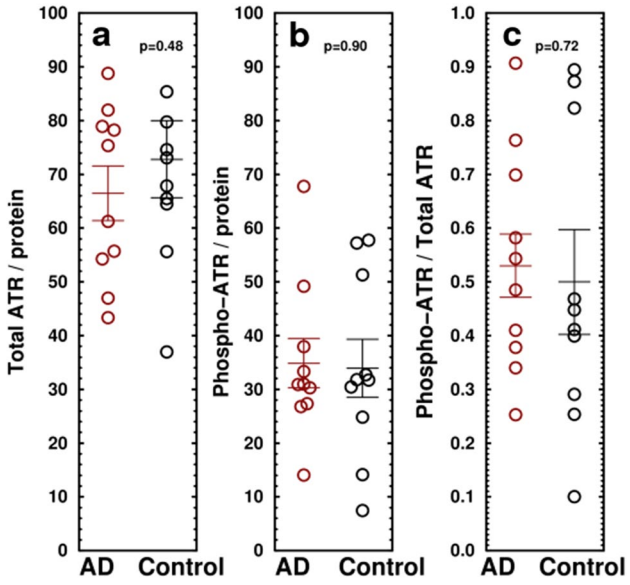

Figure 3. Changes in ATR in AD. Scatterplots show the levels of (**a**) ATR, a marker of ssDNA damage, (**b**) T1989-phosphorylated ATR, and (**c**) ratio of p-ATR to total ATR. No significant changes are evident in temporal lobe of AD patients. Measured by ELISA. This was confirmed by Western blots (Fig. S02).

of phospho(S15)-p53 in 15,000×*g* extracts using size-exclusion HPLC. Samples (0.1 min) were collected and p-p53 was measured by densitometric analysis of dot blots stained with a phospho(S15)-p53 specific antibody. Nutlin-3, an inhibitor of MDM2 (Kd = 90 nM; 300 nM used), and phosphatase/protease inhibitors were present throughout the procedure to minimize artifactual changes. The results showed a marked increase in monomeric p-p53 in AD samples compared to unaffected patients. Small amounts of tetrameric p53 in cytosol were also detectable in AD samples but not controls (Peak areas: Tetramer AD = 3.66 ± 1.41, Con = 0.95 ± 0.52, p = 0.11. Dimer: AD = 9.15 ± 2.11, Con = 6.63 ± 0.78, p = 0.29. Monomer: AD = 9.92 ± 1.73, Con = 2.99 ± 0.57, p = 0.0052; $\bar{x}$ ± SE, n = 5; Fig. 4a). These differences were not due to the presence or formation of aggregated p53, which elutes at 3.5 min (Fig. 4a inset). These results are consistent with previous studies that found that only 30% of p53 in healthy patients is monomeric[71]. However, the increased monomer fraction in AD was contrary to expectation. Native unmodified monomeric p53 tetramerizes spontaneously[72,73]. Thus, a change in oligomerization state indicates a stable structural change in p53. The monomer:dimer ratio in AD samples was 2.86 ± 0.72 × Control, N = 5, p = 0.017 (Fig. 4b), while the monomer:tetramer ratio showed no statistically significant change (Fig. 4d). Only small levels of p-p53 were detected in isolated nuclei, and no differences in nuclear p-p53 were observed on Western blots (Fig. S03), indicating that the result is not due to changes in tetramerized p53.

Incubation of control temporal lobe homogenates for 30 min with 100 nM H_2O_2 increased the monomer:dimer ratio nearly to AD levels (Fig. 4c). These are physiologically attainable levels: inflammation can raise H_2O_2 levels in neurons by 25–75x, reaching 66 nM in the case of respiratory chain stimulation by insulin in cerebellar granule neurons[74]. Thus, p53 protein oxidation is a possible explanation for the increased monomer/dimer ratio in AD. However, p53 exists in at least 9 isoforms produced by alternative splicing and is potentially subject to a large number of other post-translational modifications including ubiquitination, phosphorylation, acetylation, and methylation. We cannot rule out the possibility that these forms of p53 also exhibit differential tendencies for oligomerization.

STING is depleted from Golgi in AD. Cytosolic DNA fragments are potent inducers of interferon expression via the STING-cGAS pathway. STING protein exists in several alternatively-spliced forms[75]. In human brain, the 52 kDa wild-type and 30 kDa Isoform 1 are highly abundant. The 52 kDa isoform is translocated to Golgi in response to elevated cGAMP produced by cGAS (cGAMP synthase) after DNA damage, while the 30 kDa isoform is found only in cytosol. To determine whether the damaged DNA in AD activates the STING pathway, we used the Minute Golgi Apparatus Enrichment Kit (Invent Biotechnologies, Plymouth MN) to enrich Golgi apparatus and Golgi secretory vesicles from autopsy samples from patients with AD and controls. While little change was seen in 52 kDa and 30 kDa forms of STING in raw homogenates, cytosol, or nuclei, 52 kDa wild-type STING in Golgi fractions measured by densitometry was 2.82 ± 0.54 × lower from AD patients than controls (AD = 14.3 ± 1.18, control = 40.3 ± 6.9, $\bar{x}$ ± SE, n = 10, p = 0.0027), suggesting almost total depletion of STING in Golgi in AD (Fig. 5a). The 30 kDa cytosolic isoform was also increased in AD samples to 213 ± 55% control (p = 0.026, n = 13, Fig. 5b). No change in the 30 kDa isoform of STING was observed in secretory vesicles (Fig. 5c) and no change in the 52 kDa isoform of STING was observed in nuclei (AD = 50.8 ± 2.7, control = 51.1 ± 2.6, $\bar{x}$ ± SE, n = 10, p = 0.96; Figs. 5d,e, S04).

Consistent with this finding, the fraction of interferon-beta (IFNβ) in particulate fractions (presumed to represent predominantly receptor-bound IFN), measured by ELISA, was slightly decreased in AD

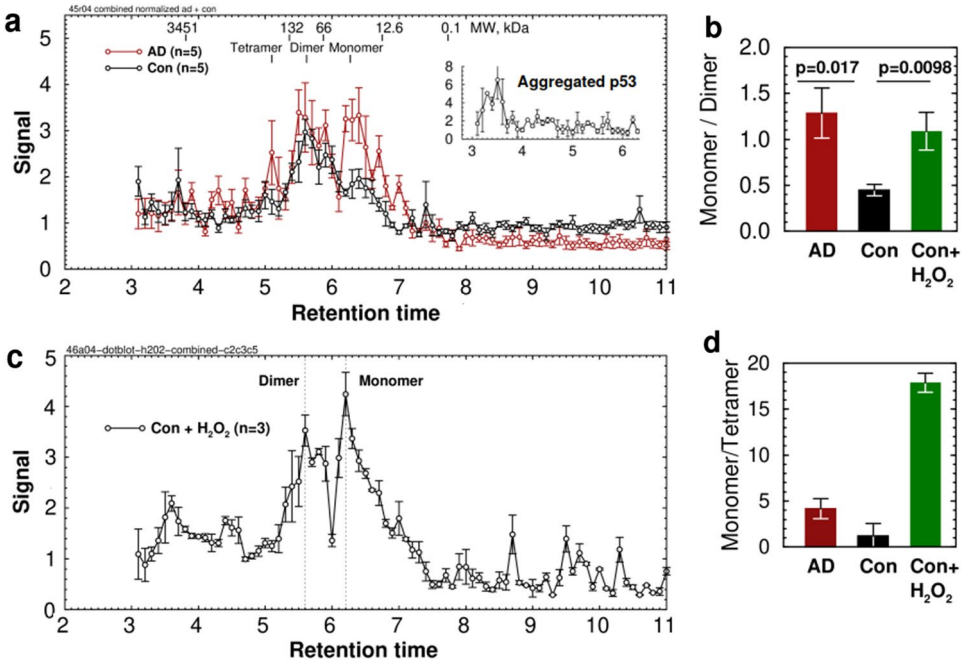

Figure 4. Phosphorylated (S15) p53 oligomerization state is changed in AD. Extracts from human AD and control temporal lobe were chromatographed on size-exclusion HPLC and analyzed by p53-pS15 dot blot followed by densitometry. (**a**) Averaged chromatograms from temporal lobe of five AD and five age-matched controls. Inset shows a chromatogram from a sample that was deliberately concentrated to induce unfolded p53 and aggregation. (**b**) Ratio of monomer/dimer peak areas calculated from the chromatograms. AD = 1.29 ± 0.27, Con = 0.45 ± 0.06, Con + H_2O_2 = 1.09 ± 0.20, $\bar{x}$ ± SEM. n = 5, AD vs. Con: p = 0.017, N = 5. (**c**) Oxidation by 100 nM hydrogen peroxide for 30 min increases p53 monomer/dimer ratio. (**d**) Ratio of monomer/tetramer peak areas calculated from the chromatograms. AD = 4.17 ± 1.10, Con = 1.22 ± 1.35, Con + H_2O_2 = 17.9 ± 1.0, n = 3, n.s.

(AD = 0.368 ± 0.017, Con = 0.435 ± 0.037, n = 10, p = 0.030) while IFNβ in cytosol was not affected in AD (2.94 ± 0.15, Con = 3.09 ± 0.26 pg/mg protein, n = 10, p = 0.62) (Fig. 6a,b). Total IFNα and membrane/total IFNα were not affected by AD (Fig. 6c,d), confirming a failure of STING to produce a significant interferon response to DNA damage. This finding is consistent with the observed depletion of wild-type 52 kDa STING from Golgi in AD samples. These results suggest that the STING-IFN pathway is compromised in AD.

IRF3 phosphorylation is decreased in AD. There is evidence that the p53 and STING pathways are interdependent. p53 knockdown prevents a type I interferon-mediated immune response to influenza virus[76], and cancer cells with constitutively inactive p53 have deficiencies in cGAS-STING signaling[77]. In cancer cells, inactive mutant p53 binds to TBK1 (TANK-binding kinase), blocking the phosphorylation of IRF3 (interferon regulatory factor 3) by TBK1 and suppressing the formation of the STING-TBK1-IRF3 trimeric complex required for interferon expression[77]. This suggests a mechanism by which the increase in p53 monomerization in AD could produce the effects on STING and interferon that we observed. Western blots (Fig. 7) showed that IRF3 phosphorylation was decreased in AD to 76.5 ± 4.5% of control (n = 18, p = 0.00016). The ratio of pIRF3/total IRF3 was also decreased (Figs. 7, S05) (AD = 0.582 ± 0.038, control = 1.131 ± 0.152, n = 11, p = 0.0030), suggesting that phosphorylation of IRF3, which is required for formation of the trimeric complex, may be inhibited in AD. Further experimentation is needed to determine whether p53 monomerization alone is sufficient to inhibit TBK1 signaling and to establish the mechanism by which p53 isoforms and post-translational modifications and oligomerization state inhibit IRF3 phosphorylation.

Discussion

These results provide evidence that the DNA damage repair (DDR) response is compromised in AD. Oxidation of p53 by ROS could affect the DDR by altering the oligomerization state of p53. Unrepaired DSBs result in somatic mutations and other catastrophic effects for a cell. Evidence suggests that the DSBs are produced in part by ROS created during inflammation by activation of non-mitochondrial[78] NADPH oxidase (NOX), which is normally inert but is activated by cytokines, angiotensin II, hypoxia, or oxidized fatty acids which are found in obesity[79–82]. Overactivation of NOX in cerebrovascular endothelial cells is one of the main causes of cerebrovascular damage in AD[83]. Apocynin, a NOX inhibitor, reduces vascular β-amyloid deposits by 80% in patients with cerebral amyloid angiopathy (CAA)[84], a co-morbidity in > 90% of AD patients. Thus, it is possible that much of the unrepaired DNA damage could be attributed to NOX activated in patients carrying risk factors for AD, including inflammation and obesity.

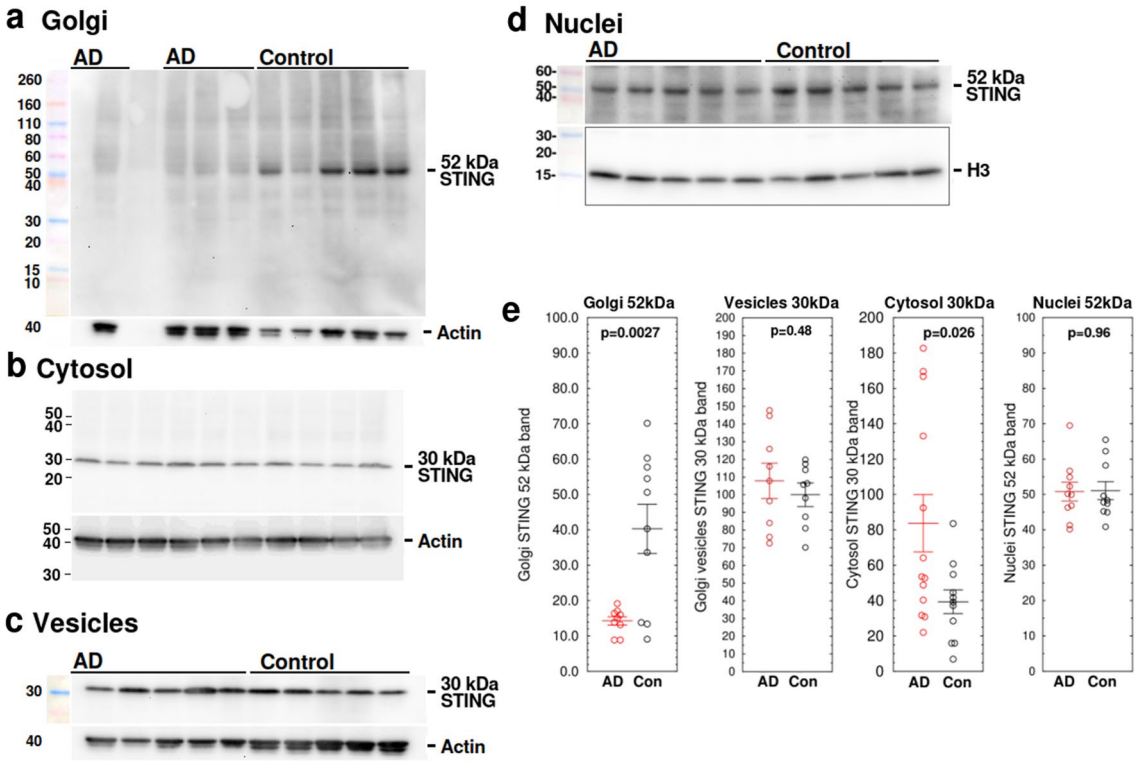

Figure 5. STING protein is depleted from Golgi in AD. (**a**) Representative Western blots of the 52 kDa isoform of STING in enriched Golgi fractions from AD and control temporal lobe, measured by densitometry. STING was 2.82 ± 0.54 × lower in AD patients than controls (AD = 14.3 ± 1.18, control = 40.3 ± 6.9, $\bar{x}$ ± SEM, n = 10, p = 0.0027). (**b**) The 30 kDa isoform of STING was moderately increased in cytosol extracted from the same samples (AD = 83.7 ± 16.2, control = 39.4 ± 6.7, n = 13, p = 0.026, $\bar{x}$ ± SEM). (**c**) Representative Western blot of 30 kDa isoform of STING protein from isolated Golgi vesicles from AD and control temporal lobe. No statistically significant change was observed. (**d**) Representative Western blot of 52 kDa isoform of STING protein from isolated nuclei from AD and control temporal lobe. No statistically significant change was observed. (**e**) Scatterplots of combined data from Western blots of 52 kDa and 30 kDa STING protein in Golgi, cytosol, and nuclei. Western blots in (**a**–**c**) and d are different blots. Blots were stripped and re-probed with actin (**a**–**c**) or histone H3 (**d**). Colored MW markers were photographed on the corresponding blot at the time of initial immunostaining. Western blot images shown have been cropped for clarity of presentation. Original full-size blots are presented in Supplementary Fig. S04a–n. Scatterplots represent combined densitometry results from 10 to 13 AD samples and an equal number of age-matched unaffected patients (Con).

Many links have been reported between DNA damage and tau neurofibrillary tangles (NFTs), which are a hallmark of AD. Extensive DNA damage as shown by the terminal deoxynucleotidyl transferase-dUTP nick end labeling (TUNEL) assay occurs in cerebral cortical neurons in AD[85,86]. This DNA damage is associated with NFTs[87] and has been attributed to neuronal vulnerability and necrosis rather than apoptosis[88,89], although some researchers also report apoptotic morphologies[90]. NFTs contain phospho-tau, an established biomarker for AD, and tauopathy may be a driver for neuron loss in AD via necroptosis, possibly involving cofactors such as Transactive Response DNA-binding protein 43 (TDP-43) and Aβ[91]. Co-expression of 3R-tau isoforms can induce oxidative DSBs along with glial activation, neuronal death, and memory deficits[92]. These effects are reversed by antioxidants[92]. Tau can also interact with p53: depletion of tau in cultured neuroblastoma cells alters p53 stability and reduces cell death[93,94]. DSBs and phospho-tau frequently co-localize in AD cortex. Knockdown of tau exacerbates DSBs in neurons, suggesting a role for tau in DNA repair[95], consistent with a role for tau in protecting neuronal genomic DNA integrity[96].

Links have also been reported between Aβ plaques and DNA damage. Aβ induces oxidative stress, in part by interfering with normal mitochondrial activity[97], and induces oxidative DNA damage[79] as shown by 8-hydroxy-2'-deoxyguanosine (8-OHdG) staining and histone phosphorylation (γ-H2AX)[98–100]. Aβ may also contribute indirectly by inhibiting NHEJ by blocking DNA-dependent protein kinase, thereby promoting oxidative DNA damage[101]. Genomic DNA damage is reported to induce neuronal production of Aβ by increasing β-secretase activity[102]. Besides immunotherapy to deplete soluble Aβ and plaques[103], a variety of treatments have been proposed to inhibit these toxic effects of Aβ, including glutamine[104], galantamine[105], antioxidants[106], and isoflavones[107]. Lesions in myelinating oligodendrocytes in gray matter[108] and damage to astrocytes[109] also correlate with DNA damage, suggesting that DNA damage in non-neuronal cells may also contribute to AD. However, cognitively healthy centenarians have NIA (amyloid) and Braak (NFT) stages similar to AD patients, suggesting that a portion of the population is cognitively resilient to AD[110,111].

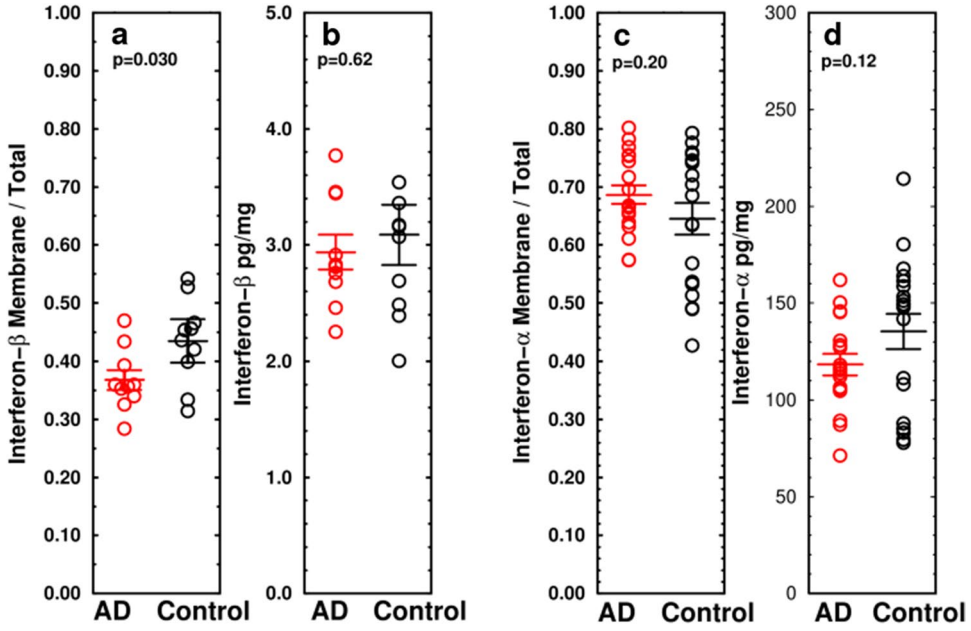

Figure 6. Total and membrane-associated interferon α and β measured by ELISA show little or no change in AD compared to control temporal lobe samples. (**a**,**b**) Membrane-associated IFNβ is moderately decreased in AD (ratio of particulate/cytosol: AD = 0.592 ± 0.045 pg/mg protein, control = 0.797 ± 0.073, p = 0.030, n = 10/group, $\bar{x} \pm$ SEM) while total IFNβ shows no effect in AD. (**c**,**d**) Membrane-associated IFNα and total IFNα do not differ between AD and unaffected patients.

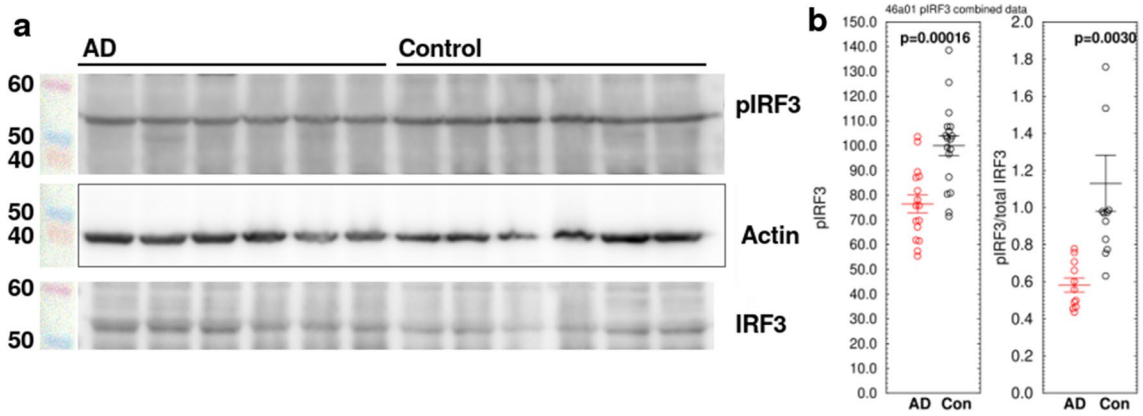

Figure 7. Phosphorylation of IRF3 is decreased in homogenates of AD temporal lobes compared to age-matched controls. (**a**) Representative Western blot. (**b**) Scatterplots of all pIRF3 samples measured by densitometry of Western blots. IRF3 phosphorylation (S396) was decreased in AD to 76.5 ± 4.5% of control (n = 18, p = 0.00016). The ratio of pIRF3/total IRF3 was also decreased (AD = 0.582 ± 0.038, control = 1.131 ± 0.152, n = 11, p = 0.0030), suggesting that phosphorylation of IRF3, which is required for formation of the trimeric complex, is inhibited in AD. All three panels are from the same blot. Western blot images shown have been cropped for clarity of presentation. Original full-size blots are presented in Supplementary Fig. S05. After imaging, the pIRF3 blot in (**a**) was stripped and re-probed for actin, then re-probed for total IRF3. Colored MW markers were photographed on the blot at the time of pIRF3 staining. Scatterplots represent combined densitometry results from 11 to 18 AD samples and an equal number of age-matched unaffected patients (Con).

The results also provide evidence that the cGAS-STING pathway, which is activated by pathogen-derived and self-DNA, mediates immune surveillance, and induces the Type I interferon response, is impaired in the temporal lobe of human patients with AD despite evidence of DSBs. Our finding that IRF3 phosphorylation is decreased in AD, combined with our finding that oligomerization of p53 is inhibited in AD, suggests that a similar mechanism could explain the observed effects on STING and interferon. However, further experimentation is necessary.

Whether p53 induces cellular senescence or apoptosis depends on its oligomerization state (Fig. 8) and a large number of potential post-translational modifications[112–117]. Phosphorylation of p53 at S15 leads to decreased

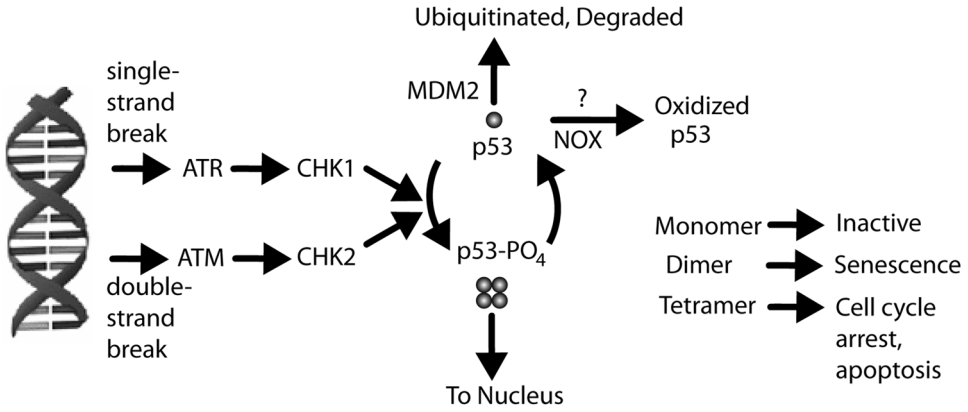

Figure 8. Role of p53 in DNA repair pathway. The DNA damage repair pathway involves activation of ATR for ssDNA breaks and ATM for dsDNA breaks. These kinases act on CHK1 and CHK2 to phosphorylate p53. Dephosphorylated p53 is ubiquitinated by MDM2 and rapidly degraded at the proteasome. Phosphorylation of p53 at S15 inhibits interaction with MDM2. p53 induces MDM2 transcription, ensuring that the lifetime of p53 is short. Phosphorylation and oligomerization state determine p53's effect so that p53 acts as a switch to control the cell's response to DNA damage. The tetramerized form most strongly binds DNA. Many other post-translational modifications of p53 have been described.

interaction with its negative regulator, MDM2[13], an E3 ubiquitin kinase that targets p53 for proteasomal degradation, leading to higher levels of p53 protein[118,119]. Phosphorylation at S15 and S20 increases p53 stability, enhances tetramerization[120], and favors senescence, while phosphorylation at S46 combined with acetylation at K382 induces apoptosis[121,122]. Conversely, NOX1 (NADPH oxidase 1) impairs p53 K382 acetylation, preventing apoptosis[123]. ROS produced during inflammation could induce the dissociation of dimeric and tetrameric p53 to the inactive monomer form and thereby inhibit DNA repair and interferon signaling. If so, shifting the redox balance could restore p53 to its active state and thereby enhance DNA repair. As mentioned above, Aβ can also induce oxidative stress, which induces DSBs. Aβ was also reported to increase expression of p53 and its transcription target, Bax, in cultured cortical neurons[124]. Upregulation of p53 by Nutlin-3 is reported to prevent Aβ42-induced DNA damage[125]. However, other studies report that inactivation of p53 has no effect on induction of apoptosis by Aβ(25–35) in cultured cells, suggesting that Aβ-induced apoptosis does not depend on p53.

The finding of impaired p53 oligomerization in AD reported here is entirely distinct from p53 misfolding or unfolding. Misfolded p53 forms amyloid-like aggregates that impair its DNA-binding function[43,126]. Misfolded p53 has been found in PBMCs[127,128] and fibroblasts[129] but not neurons[130] and has been proposed as an early marker of AD. Misfolded p53 is easily measured and elutes at 3.5 min in SEC-HPLC (Fig. 6a, insert). However, no non-artifactual unfolded p53 was observed in our CNS samples and there are no reports of it in CNS. Unfolding of p53 is unrelated to its oligomerization state[131] and can be produced when p53 is not bound to its cognate DNA[132] or when p53 is artificially concentrated in vitro. The involvement of p53 also provides a possible explanation for the long-hypothesized inverse connections between AD and cancer, recently replicated in large longitudinal studies[133–135].

While cGAS is normally thought of as an activator of STING, chronic activation of cGAS by persistent unrepaired DNA damage can also induce STING to undergo a phase transition to a membranous condensate that isolates STING from its effector protein IRF3[136,137]. Thus, depletion of STING from Golgi in AD patients, and hence loss of interferon responses, could be a response to chronic DNA damage. The cortex is composed primarily of neurons, and we cannot rule out a similar or compensatory effect in glial cells. Impaired interferon responses would increase the risk of AD progression[138] and drive microglial dysfunction[139].

Antioxidants have been proposed many times as general nonspecific treatments for oxidative stress in AD. However, designing effective antioxidant therapies specific for AD requires knowledge of specific targets and mechanisms in AD. p53 activity and tetramerization are strongly dependent on redox factor 1 (Ref-1/APE1), a protein involved in base excision repair, and thioredoxin, which reactivates oxidized p53[140–143]. Thus, elevating thioredoxin levels could be another potential way of restoring DNA repair in AD.

Data availability

The datasets generated during and/or analyzed during the current study are available from the corresponding author on reasonable request.

Code availability

Source code and related files for the software used in data analysis are available from the corresponding author on reasonable request.

Received: 10 February 2023; Accepted: 19 May 2023
Published online: 23 May 2023

References

1. Vemuri, P. *et al.* Evaluation of amyloid protective factors and Alzheimer disease neurodegeneration protective factors in elderly individuals. *JAMA Neurol.* **74**(6), 718–726. https://doi.org/10.1001/jamaneurol.2017.0244 (2017) (**Epub 2017/04/19**).
2. Soheili-Nezhad, S., van der Linden, R. J., Olde Rikkert, M., Sprooten, E. & Poelmans, G. Long genes are more frequently affected by somatic mutations and show reduced expression in Alzheimer's disease: Implications for disease etiology. *Alzheimer's Dementia* **17**(3), 489–499. https://doi.org/10.1002/alz.12211 (2021) (**Epub 2020/10/20**).
3. Thadathil, N. *et al.* DNA Double-strand break accumulation in Alzheimer's disease: Evidence from experimental models and postmortem human brains. *Mol. Neurobiol.* **58**(1), 118–131. https://doi.org/10.1007/s12035-020-02109-8 (2021) (**Epub 2020/09/09**).
4. Bussian, T. J. *et al.* Clearance of senescent glial cells prevents tau-dependent pathology and cognitive decline. *Nature* **562**(7728), 578–582. https://doi.org/10.1038/s41586-018-0543-y (2018) (**Epub 2018/09/21**).
5. Baker, D. J. & Petersen, R. C. Cellular senescence in brain aging and neurodegenerative diseases: Evidence and perspectives. *J. Clin. Investig.* **128**(4), 1208–1216. https://doi.org/10.1172/jci95145 (2018) (**Epub 2018/02/20**).
6. Coppedè, F. & Migliore, L. DNA damage in neurodegenerative diseases. *Mutat. Res.* **776**, 84–97. https://doi.org/10.1016/j.mrfmmm.2014.11.010 (2015) (**Epub 2015/08/11**).
7. Madabhushi, R., Pan, L. & Tsai, L. H. DNA damage and its links to neurodegeneration. *Neuron* **83**(2), 266–282. https://doi.org/10.1016/j.neuron.2014.06.034 (2014) (**Epub 2014/07/18**).
8. Simpson, J. E. *et al.* A neuronal DNA damage response is detected at the earliest stages of Alzheimer's neuropathology and correlates with cognitive impairment in the Medical Research Council's Cognitive Function and Ageing Study ageing brain cohort. *Neuropathol. Appl. Neurobiol.* **41**(4), 483–496. https://doi.org/10.1111/nan.12202 (2015) (**Epub 2014/12/03**).
9. Lee, M. H. *et al.* Somatic APP gene recombination in Alzheimer's disease and normal neurons. *Nature* **563**(7733), 639–645. https://doi.org/10.1038/s41586-018-0718-6 (2018) (**Epub 2018/11/23**).
10. Miller, M. B., Reed, H. C. & Walsh, C. A. Brain somatic mutation in aging and Alzheimer's disease. *Annu. Rev. Genomics Hum. Genet.* https://doi.org/10.1146/annurev-genom-121520-081242 (2021) (**Epub 2021/05/13**).
11. Tian, B., Yang, Q. & Mao, Z. Phosphorylation of ATM by Cdk5 mediates DNA damage signalling and regulates neuronal death. *Nat. Cell Biol.* **11**(2), 211–218. https://doi.org/10.1038/ncb1829 (2009) (**Epub 2009/01/20**).
12. Goikolea, J. *et al.* Serum Thioredoxin-80 is associated with age, ApoE4, and neuropathological biomarkers in Alzheimer's disease: A potential early sign of AD. *Alzheimer's Res. Ther.* **14**(1), 37. https://doi.org/10.1186/s13195-022-00979-9 (2022) (**Epub 2022/02/26**).
13. Shieh, S. Y., Ikeda, M., Taya, Y. & Prives, C. DNA damage-induced phosphorylation of p53 alleviates inhibition by MDM2. *Cell* **91**(3), 325–334. https://doi.org/10.1016/s0092-8674(00)80416-x (1997) (**Epub 1997/11/18**).
14. Mohammadzadeh, A. *et al.* Crosstalk between P53 and DNA damage response in ageing. *DNA Repair* **80**, 8–15. https://doi.org/10.1016/j.dnarep.2019.05.004 (2019) (**Epub 2019/06/10**).
15. White, R. R. *et al.* Controlled induction of DNA double-strand breaks in the mouse liver induces features of tissue ageing. *Nat. Commun.* **6**(1), 6790. https://doi.org/10.1038/ncomms7790 (2015).
16. Li, H., Mitchell, J. R. & Hasty, P. DNA double-strand breaks: A potential causative factor for mammalian aging?. *Mech Ageing Dev.* **129**(7–8), 416–424. https://doi.org/10.1016/j.mad.2008.02.002 (2008) (**Epub 2008/03/19**).
17. Lans, H. & Hoeijmakers, J. H. Genome stability, progressive kidney failure and aging. *Nat. Genet.* **44**(8), 836–838. https://doi.org/10.1038/ng.2363 (2012) (**Epub 2012/07/28**).
18. Oster, S. & Aqeilan, R. I. Programmed DNA damage and physiological DSBs: Mapping, biological significance and perturbations in disease states. *Cells* https://doi.org/10.3390/cells9081870 (2020) (**Epub 2020/08/14**).
19. Sallmyr, A. & Tomkinson, A. E. Repair of DNA double-strand breaks by mammalian alternative end-joining pathways. *J. Biol. Chem.* **293**(27), 10536–10546. https://doi.org/10.1074/jbc.TM117.000375 (2018).
20. Ferreira, S. T., Clarke, J. R., Bomfim, T. R. & De Felice, F. G. Inflammation, defective insulin signaling, and neuronal dysfunction in Alzheimer's disease. *Alzheimer's Dementia* **10**(1 Suppl), S76-83. https://doi.org/10.1016/j.jalz.2013.12.010 (2014) (**Epub 2014/02/18**).
21. Banks, W. A. Blood-brain barrier transport of cytokines: A mechanism for neuropathology. *Curr. Pharm. Des.* **11**(8), 973–984. https://doi.org/10.2174/1381612053381684 (2005) (**Epub 2005/03/22**).
22. Pan, W. & Kastin, A. J. Interactions of cytokines with the blood–brain barrier: Implications for feeding. *Curr. Pharm. Des.* **9**(10), 827–831. https://doi.org/10.2174/1381612033455332 (2003) (**Epub 2003/04/08**).
23. Chen, K. & Keaney, J. F. Jr. Evolving concepts of oxidative stress and reactive oxygen species in cardiovascular disease. *Curr. Atheroscler. Rep.* **14**(5), 476–483. https://doi.org/10.1007/s11883-012-0266-8 (2012) (**Epub 2012/09/08**).
24. Guedj, A. *et al.* Gut microbiota shape "inflamm-ageing" cytokines and account for age-dependent decline in DNA damage repair. *Gut* **69**(6), 1064–1075. https://doi.org/10.1136/gutjnl-2019-318491 (2020) (**Epub 2019/10/07**).
25. Jaiswal, M., LaRusso, N. F., Burgart, L. J. & Gores, G. J. Inflammatory cytokines induce DNA damage and inhibit DNA repair in cholangiocarcinoma cells by a nitric oxide-dependent mechanism. *Can. Res.* **60**(1), 184–190 (2000) (**Epub 2000/01/26**).
26. Tucsek, Z. *et al.* Obesity in aging exacerbates blood-brain barrier disruption, neuroinflammation, and oxidative stress in the mouse hippocampus: Effects on expression of genes involved in beta-amyloid generation and Alzheimer's disease. *J. Gerontol. A Biol. Sci. Med. Sci.* **69**(10), 1212–1226. https://doi.org/10.1093/gerona/glt177 (2014) (**Epub 2013/11/26**).
27. Bryant, A. G. *et al.* Cerebrovascular senescence is associated with tau pathology in Alzheimer's disease. *Front. Neurol.* **11**, 575953. https://doi.org/10.3389/fneur.2020.575953 (2020) (**Epub 2020/10/13**).
28. Lyons, C. E. & Bartolomucci, A. Stress and Alzheimer's disease: A senescence link?. *Neurosci. Biobehav. Rev.* **115**, 285–298. https://doi.org/10.1016/j.neubiorev.2020.05.010 (2020) (**Epub 2020/05/29**).
29. Masaldan, S., Belaidi, A. A., Ayton, S. & Bush, A. I. Cellular senescence and iron dyshomeostasis in Alzheimer's disease. *Pharmaceuticals* https://doi.org/10.3390/ph12020093 (2019) (**Epub 2019/06/30**).
30. Zhang, P. *et al.* Senolytic therapy alleviates Aβ-associated oligodendrocyte progenitor cell senescence and cognitive deficits in an Alzheimer's disease model. *Nat. Neurosci.* **22**(5), 719–728. https://doi.org/10.1038/s41593-019-0372-9 (2019) (**Epub 2019/04/03**).
31. Ohyagi, Y. *et al.* Intracellular Abeta42 activates p53 promoter: A pathway to neurodegeneration in Alzheimer's disease. *FASEB J.* **19**(2), 255–257. https://doi.org/10.1096/fj.04-2637fje (2005) (**Epub 2004/11/19**).
32. Shi, D. & Jiang, P. A different facet of p53 function: Regulation of immunity and inflammation during tumor development. *Front. Cell Dev. Biol.* **9**, 762651. https://doi.org/10.3389/fcell.2021.762651 (2021) (**Epub 2021/11/05**).
33. Musi, N. *et al.* Tau protein aggregation is associated with cellular senescence in the brain. *Aging Cell* **17**(6), e12840. https://doi.org/10.1111/acel.12840 (2018) (**Epub 2018/08/21**).
34. Sikora, E. *et al.* Cellular senescence in brain aging. *Front. Aging Neurosci.* **13**, 646924. https://doi.org/10.3389/fnagi.2021.646924 (2021) (**Epub 2021/03/19**).
35. Amor-Gutiérrez, O. *et al.* Competitive electrochemical immunosensor for the detection of unfolded p53 protein in blood as biomarker for Alzheimer's disease. *Anal. Chim. Acta* **1093**, 28–34. https://doi.org/10.1016/j.aca.2019.09.042 (2020) (**Epub 2019/11/19**).
36. Buizza, L. *et al.* Conformational altered p53 as an early marker of oxidative stress in Alzheimer's disease. *PLoS ONE* **7**(1), e29789. https://doi.org/10.1371/journal.pone.0029789 (2012) (**Epub 2012/01/14**).

37. Zhou, X. & Jia, J. P53-mediated G(1)/S checkpoint dysfunction in lymphocytes from Alzheimer's disease patients. *Neurosci. Lett.* **468**(3), 320–325. https://doi.org/10.1016/j.neulet.2009.11.024 (2010) (**Epub 2009/11/17**).
38. Arce-Varas, N. *et al.* Comparison of extracellular and intracellular blood compartments highlights redox alterations in Alzheimer's and mild cognitive impairment patients. *Curr. Alzheimer Res.* **14**(1), 112–122. https://doi.org/10.2174/1567205013666161010125413 (2017) (**Epub 2016/10/18**).
39. Abate, G. *et al.* A Conformation variant of p53 combined with machine learning identifies Alzheimer disease in preclinical and prodromal stages. *J. Pers. Med.* https://doi.org/10.3390/jpm11010014 (2020) (**Epub 2020/12/31**).
40. Stanga, S. *et al.* Unfolded p53 in the pathogenesis of Alzheimer's disease: Is HIPK2 the link?. *Aging* **2**(9), 545–554. https://doi.org/10.18632/aging.100205 (2010) (**Epub 2010/09/30**).
41. Lanni, C. *et al.* Unfolded p53 in blood as a predictive signature signature of the transition from mild cognitive impairment to Alzheimer's disease. *J. Alzheimers Dis.* **20**(1), 97–104. https://doi.org/10.3233/jad-2010-1347 (2010) (**Epub 2010/02/19**).
42. Uberti, D., Lanni, C., Racchi, M., Govoni, S. & Memo, M. Conformationally altered p53: A putative peripheral marker for Alzheimer's disease. *Neurodegener. Dis.* **5**(3–4), 209–211. https://doi.org/10.1159/000113704 (2008) (**Epub 2008/03/07**).
43. Uberti, D. *et al.* Identification of a mutant-like conformation of p53 in fibroblasts from sporadic Alzheimer's disease patients. *Neurobiol. Aging.* **27**(9), 1193–1201. https://doi.org/10.1016/j.neurobiolaging.2005.06.013 (2006) (**Epub 2005/09/17**).
44. Zand, H. *et al.* Obesity-induced p53 activation in insulin-dependent and independent tissues is inhibited by beta-adrenergic agonist in diet-induced obese rats. *Life Sci.* **147**, 103–109. https://doi.org/10.1016/j.lfs.2016.01.040 (2016) (**Epub 2016/02/02**).
45. Liu, S., Kim, T. H., Franklin, D. A. & Zhang, Y. Protection against High-fat-diet-induced obesity in MDM2(C305F) mice due to reduced p53 activity and enhanced energy expenditure. *Cell Rep.* **18**(4), 1005–1018. https://doi.org/10.1016/j.celrep.2016.12.086 (2017) (**Epub 2017/01/26**).
46. Yu, H., Harrison, F. E. & Xia, F. Altered DNA repair; an early pathogenic pathway in Alzheimer's disease and obesity. *Sci. Rep.* **8**(1), 5600. https://doi.org/10.1038/s41598-018-23644-4 (2018) (**Epub 2018/04/06**).
47. Azzarà, A. *et al.* Increased level of DNA damage in some organs of obese Zucker rats by γ-H2AX analysis. *Environ. Mol. Mutagen.* **58**(7), 477–484. https://doi.org/10.1002/em.22115 (2017) (**Epub 2017/07/18**).
48. Scarpato, R. *et al.* Nuclear damage in peripheral lymphocytes of obese and overweight Italian children as evaluated by the gamma-H2AX focus assay and micronucleus test. *FASEB J.* **25**(2), 685–693. https://doi.org/10.1096/fj.10-168427 (2011) (**Epub 2010/11/12**).
49. Storozynsky, Q. & Hitt, M. M. The impact of radiation-induced DNA damage on cGAS-STING-mediated immune responses to cancer. *Int. J. Mol. Sci.* https://doi.org/10.3390/ijms21228877 (2020) (**Epub 2020/11/27**).
50. Hu, X. *et al.* Emerging role of STING signalling in CNS injury: Inflammation, autophagy, necroptosis, ferroptosis and pyroptosis. *J. Neuroinflamm.* **19**(1), 242. https://doi.org/10.1186/s12974-022-02602-y (2022) (**Epub 2022/10/05**).
51. Glück, S. *et al.* Innate immune sensing of cytosolic chromatin fragments through cGAS promotes senescence. *Nat. Cell Biol.* **19**(9), 1061–1070. https://doi.org/10.1038/ncb3586 (2017) (**Epub 2017/08/02**).
52. Dou, Z. *et al.* Cytoplasmic chromatin triggers inflammation in senescence and cancer. *Nature* **550**(7676), 402–406. https://doi.org/10.1038/nature24050 (2017) (**Epub 2017/10/05**).
53. Ablasser, A. & Chen, Z. J. cGAS in action: Expanding roles in immunity and inflammation. *Science* https://doi.org/10.1126/science.aat8657 (2019) (**Epub 2019/03/09**).
54. Qiu, Z. *et al.* Programmed death of microglia in Alzheimer's disease: Autophagy, ferroptosis, and pyroptosis. *J. Prev. Alzheimers Dis.* **10**(1), 95–103. https://doi.org/10.14283/jpad.2023.3 (2023) (**Epub 2023/01/16**).
55. Torres-Perez, E., Ledesma, M., Garcia-Sobreviela, M. P., Leon-Latre, M. & Arbones-Mainar, J. M. Apolipoprotein E4 association with metabolic syndrome depends on body fatness. *Atherosclerosis* **245**, 35–42. https://doi.org/10.1016/j.atherosclerosis.2015.11.029 (2016) (**Epub 2015/12/23**).
56. Collins, A. R. The comet assay for DNA damage and repair: Principles, applications, and limitations. *Mol. Biotechnol.* **26**(3), 249–261. https://doi.org/10.1385/mb:26:3:249 (2004) (**Epub 2004/03/09**).
57. Ishida, R. *et al.* GM130 is a parallel tetramer with a flexible rod-like structure and N-terminally open (Y-shaped) and closed (I-shaped) conformations. *FEBS J.* **282**(11), 2232–2244. https://doi.org/10.1111/febs.13271 (2015) (**Epub 2015/03/20**).
58. Hooper, C. *et al.* p53 is upregulated in Alzheimer's disease and induces tau phosphorylation in HEK293a cells. *Neurosci. Lett.* **418**(1), 34–37. https://doi.org/10.1016/j.neulet.2007.03.026 (2007) (**Epub 2007/04/03**).
59. Farmer, K. M. *et al.* P53 aggregation, interactions with tau, and impaired DNA damage response in Alzheimer's disease. *Acta Neuropathol. Commun.* **8**(1), 132. https://doi.org/10.1186/s40478-020-01012-6 (2020) (**Epub 2020/08/12**).
60. Cenini, G., Sultana, R., Memo, M. & Butterfield, D. A. Elevated levels of pro-apoptotic p53 and its oxidative modification by the lipid peroxidation product, HNE, in brain from subjects with amnestic mild cognitive impairment and Alzheimer's disease. *J. Cell Mol. Med.* **12**(3), 987–994. https://doi.org/10.1111/j.1582-4934.2008.00163.x (2008) (**Epub 2008/05/23**).
61. de la Monte, S. M., Sohn, Y. K. & Wands, J. R. Correlates of p53- and Fas (CD95)-mediated apoptosis in Alzheimer's disease. *J. Neurol. Sci.* **152**(1), 73–83. https://doi.org/10.1016/s0022-510x(97)00131-7 (1997) (**Epub 1997/12/12**).
62. Kitamura, Y. *et al.* Changes of p53 in the brains of patients with Alzheimer's disease. *Biochem. Biophys. Res. Commun.* **232**(2), 418–421. https://doi.org/10.1006/bbrc.1997.6301 (1997) (**Epub 1997/03/17**).
63. Frohnert, B. I. *et al.* Increased adipose protein carbonylation in human obesity. *Obesity* **19**(9), 1735–1741. https://doi.org/10.1038/oby.2011.115 (2011) (**Epub 2011/05/20**).
64. Hauck, A. K. *et al.* Obesity-induced protein carbonylation in murine adipose tissue regulates the DNA-binding domain of nuclear zinc finger proteins. *J. Biol. Chem.* **293**(35), 13464–13476. https://doi.org/10.1074/jbc.RA118.003469 (2018) (**Epub 2018/07/18**).
65. Sanchez-Roman, I. *et al.* Molecular markers of DNA repair and brain metabolism correlate with cognition in centenarians. *Geroscience.* **44**(1), 103–125. https://doi.org/10.1007/s11357-021-00502-2 (2022) (**Epub 2021/12/31**).
66. Cabiscol, E., Tamarit, J. & Ros, J. Protein carbonylation: Proteomics, specificity and relevance to aging. *Mass Spectrom. Rev.* **33**(1), 21–48. https://doi.org/10.1002/mas.21375 (2014) (**Epub 2013/10/12**).
67. Yang, H. Y., Wen, Y. Y., Chen, C. H., Lozano, G. & Lee, M. H. 14–3-3 sigma positively regulates p53 and suppresses tumor growth. *Mol. Cell. Biol.* **23**(20), 7096–7107. https://doi.org/10.1128/mcb.23.20.7096-7107.2003 (2003) (**Epub 2003/10/01**).
68. Rajagopalan, S., Jaulent, A. M., Wells, M., Veprintsev, D. B. & Fersht, A. R. 14–3-3 activation of DNA binding of p53 by enhancing its association into tetramers. *Nucleic Acids Res.* **36**(18), 5983–5991. https://doi.org/10.1093/nar/gkn598 (2008) (**Epub 2008/09/25**).
69. Webley, K. *et al.* Posttranslational modifications of p53 in replicative senescence overlapping but distinct from those induced by DNA damage. *Mol. Cell. Biol.* **20**(8), 2803–2808. https://doi.org/10.1128/mcb.20.8.2803-2808.2000 (2000) (**Epub 2000/03/25**).
70. Pilch, D. R. *et al.* Characteristics of gamma-H2AX foci at DNA double-strand breaks sites. *Biochem. Cell Biol.* **81**(3), 123–129. https://doi.org/10.1139/o03-042 (2003) (**Epub 2003/08/05**).
71. Gaglia, G., Guan, Y., Shah, J. V. & Lahav, G. Activation and control of p53 tetramerization in individual living cells. *Proc. Natl. Acad. Sci. USA.* **110**(38), 15497–15501. https://doi.org/10.1073/pnas.1311126110 (2013) (**Epub 2013/09/06**).
72. Mateu, M. G. & Fersht, A. R. Nine hydrophobic side chains are key determinants of the thermodynamic stability and oligomerization status of tumour suppressor p53 tetramerization domain. *EMBO J.* **17**(10), 2748–2758. https://doi.org/10.1093/emboj/17.10.2748 (1998) (**Epub 1998/06/10**).

73. Brokx, R. D., Bolewska-Pedyczak, E. & Gariépy, J. A stable human p53 heterotetramer based on constructive charge interactions within the tetramerization domain. *J. Biol. Chem.* **278**(4), 2327–2332. https://doi.org/10.1074/jbc.M208528200 (2003) (**Epub 2002/11/16**).
74. Storozhevykh, T. P., Senilova, Y. E., Persiyantseva, N. A., Pinelis, V. G. & Pomytkin, I. A. Mitochondrial respiratory chain is involved in insulin-stimulated hydrogen peroxide production and plays an integral role in insulin receptor autophosphorylation in neurons. *BMC Neurosci.* **8**, 84. https://doi.org/10.1186/1471-2202-8-84 (2007) (**Epub 2007/10/09**).
75. Rodríguez-García, E. *et al.* TMEM173 alternative spliced isoforms modulate viral replication through the STING pathway. *Immunohorizons.* **2**(11), 363–376. https://doi.org/10.4049/immunohorizons.1800068 (2018) (**Epub 2019/04/27**).
76. Zhu, Z. *et al.* Type I interferon-mediated immune response against influenza A virus is attenuated in the absence of p53. *Biochem. Biophys. Res. Commun.* **454**(1), 189–195. https://doi.org/10.1016/j.bbrc.2014.10.067 (2014) (**Epub 2014/12/03**).
77. Ghosh, M. *et al.* Mutant p53 suppresses innate immune signaling to promote tumorigenesis. *Cancer Cell* **39**(4), 494-508.e5. https://doi.org/10.1016/j.ccell.2021.01.003 (2021) (**Epub 2021/02/06**).
78. Trifunovic, A. *et al.* Premature ageing in mice expressing defective mitochondrial DNA polymerase. *Nature* **429**(6990), 417–423. https://doi.org/10.1038/nature02517 (2004) (**Epub 2004/05/28**).
79. Jang, J. H. & Surh, Y. J. beta-Amyloid induces oxidative DNA damage and cell death through activation of c-Jun N terminal kinase. *Ann. N. Y. Acad. Sci.* **973**, 228–236. https://doi.org/10.1111/j.1749-6632.2002.tb04639.x (2002) (**Epub 2002/12/18**).
80. Mao, P. & Reddy, P. H. Aging and amyloid beta-induced oxidative DNA damage and mitochondrial dysfunction in Alzheimer's disease: Implications for early intervention and therapeutics. *Biochim. Biophys. Acta.* **1812**(11), 1359–1370. https://doi.org/10.1016/j.bbadis.2011.08.005 (2011) (**Epub 2011/08/30**).
81. Colas, J. *et al.* Neuroprotection against amyloid-β-induced DNA double-strand breaks is mediated by multiple retinoic acid-dependent pathways. *Neural. Plast.* **2020**, 9369815. https://doi.org/10.1155/2020/9369815 (2020) (**Epub 2020/04/08**).
82. Suberbielle, E. *et al.* Physiologic brain activity causes DNA double-strand breaks in neurons, with exacerbation by amyloid-β. *Nat. Neurosci.* **16**(5), 613–621. https://doi.org/10.1038/nn.3356 (2013) (**Epub 2013/03/26**).
83. Tarafdar, A. & Pula, G. The role of NADPH oxidases and oxidative stress in neurodegenerative disorders. *Int. J. Mol. Sci.* https://doi.org/10.3390/ijms19123824 (2018) (**Epub 2018/12/06**).
84. Han, B. H. *et al.* Contribution of reactive oxygen species to cerebral amyloid angiopathy, vasomotor dysfunction, and microhemorrhage in aged Tg2576 mice. *Proc. Natl. Acad. Sci. USA.* **112**(8), E881–E890. https://doi.org/10.1073/pnas.1414930112 (2015) (**Epub 2015/02/13**).
85. Lassmann, H. *et al.* Cell death in Alzheimer's disease evaluated by DNA fragmentation in situ. *Acta Neuropathol.* **89**(1), 35–41. https://doi.org/10.1007/bf00294257 (1995) (**Epub 1995/01/01**).
86. Anderson, A. J., Su, J. H. & Cotman, C. W. DNA damage and apoptosis in Alzheimer's disease: Colocalization with c-Jun immunoreactivity, relationship to brain area, and effect of postmortem delay. *J. Neurosci.* **16**(5), 1710–1719. https://doi.org/10.1523/jneurosci.16-05-01710.1996 (1996) (**Epub 1996/03/01**).
87. Sheng, J. G., Mrak, R. E. & Griffin, W. S. Progressive neuronal DNA damage associated with neurofibrillary tangle formation in Alzheimer disease. *J. Neuropathol. Exp. Neurol.* **57**(4), 323–328. https://doi.org/10.1097/00005072-199804000-00003 (1998) (**Epub 1998/05/26**).
88. Stadelmann, C., Brück, W., Bancher, C., Jellinger, K. & Lassmann, H. Alzheimer disease: DNA fragmentation indicates increased neuronal vulnerability, but not apoptosis. *J. Neuropathol. Exp. Neurol.* **57**(5), 456–464. https://doi.org/10.1097/00005072-199805000-00009 (1998) (**Epub 1998/05/22**).
89. Velez-Pardo, C., Lopera, F. & Jimenez Del Rio, M. DNA damage does not correlate with amyloid-beta-plaques and neurofibrillary tangles in familial Alzheimer's disease presenilin-1 [E280A] mutation. *J. Alzheimers Dis.* **2**(1), 47–57. https://doi.org/10.3233/jad-2000-2106 (2000) (**Epub 2002/09/06**).
90. Anderson, A. J., Stoltzner, S., Lai, F., Su, J. & Nixon, R. A. Morphological and biochemical assessment of DNA damage and apoptosis in Down syndrome and Alzheimer disease, and effect of postmortem tissue archival on TUNEL. *Neurobiol. Aging.* **21**(4), 511–524. https://doi.org/10.1016/s0197-4580(00)00126-3 (2000) (**Epub 2000/08/05**).
91. Thal, D. R. & Tomé, S. O. The central role of tau in Alzheimer's disease: From neurofibrillary tangle maturation to the induction of cell death. *Brain Res. Bull.* **190**, 204–217. https://doi.org/10.1016/j.brainresbull.2022.10.006 (2022) (**Epub 2022/10/17**).
92. Xu, C. *et al.* Co-expression of three wild-type 3R-tau isoforms induces memory deficit via oxidation-related DNA damage and cell death: A promising model for tauopathies. *J. Alzheimers Dis.* **73**(3), 1105–1123. https://doi.org/10.3233/jad-191132 (2020) (**Epub 2019/12/31**).
93. Sola, M. *et al.* Tau affects P53 function and cell fate during the DNA damage response. *Commun. Biol.* **3**(1), 245. https://doi.org/10.1038/s42003-020-0975-4 (2020) (**Epub 2020/05/20**).
94. Colnaghi, L., Rondelli, D., Muzi-Falconi, M. & Sertic, S. Tau and DNA Damage in Neurodegeneration. *Brain Sci.* https://doi.org/10.3390/brainsci10120946 (2020) (**Epub 2020/12/11**).
95. Asada-Utsugi, M. *et al.* Failure of DNA double-strand break repair by tau mediates Alzheimer's disease pathology in vitro. *Commun. Biol.* **5**(1), 358. https://doi.org/10.1038/s42003-022-03312-0 (2022) (**Epub 2022/04/15**).
96. Violet, M. *et al.* A major role for Tau in neuronal DNA and RNA protection in vivo under physiological and hyperthermic conditions. *Front. Cell Neurosci.* **8**, 84. https://doi.org/10.3389/fncel.2014.00084 (2014) (**Epub 2014/03/29**).
97. Bhatia, V. & Sharma, S. Role of mitochondrial dysfunction, oxidative stress and autophagy in progression of Alzheimer's disease. *J. Neurol. Sci.* **421**, 117253. https://doi.org/10.1016/j.jns.2020.117253 (2021) (**Epub 2021/01/22**).
98. Wiatrak, B., Mieszała, P. & Gąsiorowski, K. Impact of NMDA receptor activation on DNA damage in PC12 neuron-like cell cultures in the presence of β-amyloid peptides. *Mol. Biol. Rep.* https://doi.org/10.1007/s11033-022-07856-6 (2022) (**Epub 2022/09/16**).
99. Li, Y., Lu, J., Hou, Y., Huang, S. & Pei, G. Alzheimer's amyloid-β accelerates human neuronal cell senescence which could be rescued by sirtuin-1 and aspirin. *Front. Cell Neurosci.* **16**, 906270. https://doi.org/10.3389/fncel.2022.906270 (2022) (**Epub 2022/07/06**).
100. Ungerleider, K. *et al.* Δ133p53α protects human astrocytes from amyloid-beta induced senescence and neurotoxicity. *Neuroscience* **498**, 190–202. https://doi.org/10.1016/j.neuroscience.2022.06.004 (2022) (**Epub 2022/06/19**).
101. Cardinale, A. *et al.* Sublethal doses of β-amyloid peptide abrogate DNA-dependent protein kinase activity. *J. Biol. Chem.* **287**(4), 2618–2631. https://doi.org/10.1074/jbc.M111.276550 (2012) (**Epub 2011/12/06**).
102. Das, H., Sarkar, S., Paidi, R. K. & Biswas, S. C. Subtle genomic DNA damage induces intraneuronal production of amyloid-β (1–42) by increasing β-secretase activity. *FASEB J.* **35**(5), e21569. https://doi.org/10.1096/fj.202001676RR (2021) (**Epub 2021/04/18**).
103. Sevigny, J. *et al.* The antibody aducanumab reduces Aβ plaques in Alzheimer's disease. *Nature* **537**(7618), 50–56. https://doi.org/10.1038/nature19323 (2016) (**Epub 2016/09/02**).
104. Chen, J. & Herrup, K. Glutamine acts as a neuroprotectant against DNA damage, beta-amyloid and H2O2-induced stress. *PLoS ONE* **7**(3), e33177. https://doi.org/10.1371/journal.pone.0033177 (2012) (**Epub 2012/03/14**).
105. Castillo, W. O. & Aristizabal-Pachon, A. F. Galantamine protects against beta amyloid peptide-induced DNA damage in a model for Alzheimer's disease. *Neural. Regen. Res.* **12**(6), 916–917. https://doi.org/10.4103/1673-5374.208572 (2017) (**Epub 2017/08/02**).

106. Braidy, N. *et al.* The precursor to glutathione (GSH), γ-glutamylcysteine (GGC), can ameliorate oxidative damage and neuroinflammation induced by Aβ(40) oligomers in human astrocytes. *Front. Aging Neurosci.* **11**, 177. https://doi.org/10.3389/fnagi.2019.00177 (2019) (**Epub 2019/08/24**).
107. Ma, W. W. *et al.* Genistein alleviates the mitochondria-targeted DNA damage induced by β-amyloid peptides 25–35 in C6 glioma cells. *Neurochem. Res.* **38**(7), 1315–1323. https://doi.org/10.1007/s11064-013-1019-y (2013) (**Epub 2013/03/23**).
108. Tse, K. H., Cheng, A., Ma, F. & Herrup, K. DNA damage-associated oligodendrocyte degeneration precedes amyloid pathology and contributes to Alzheimer's disease and dementia. *Alzheimer's Dementia* **14**(5), 664–679. https://doi.org/10.1016/j.jalz.2017.11.010 (2018) (**Epub 2018/01/13**).
109. Simpson, J. E. *et al.* Population variation in oxidative stress and astrocyte DNA damage in relation to Alzheimer-type pathology in the ageing brain. *Neuropathol. Appl. Neurobiol.* **36**(1), 25–40. https://doi.org/10.1111/j.1365-2990.2009.01030.x (2010) (**Epub 2009/05/09**).
110. Zhang, M. *et al.* Resilience and resistance to the accumulation of amyloid plaques and neurofibrillary tangles in centenarians: An age-continuous perspective. *Alzheimer's Dementia*. https://doi.org/10.1002/alz.12899 (2022) (**Epub 2022/12/31**).
111. Eissman, J. M. *et al.* Sex differences in the genetic architecture of cognitive resilience to Alzheimer's disease. *Brain* **145**(7), 2541–2554. https://doi.org/10.1093/brain/awac177 (2022) (**Epub 2022/05/14**).
112. d'Adda di Fagagna, F. Living on a break: Cellular senescence as a DNA-damage response. *Nat. Rev. Cancer.* **8**(7), 512–522. https://doi.org/10.1038/nrc2440 (2008) (**Epub 2008/06/25**).
113. Carlessi, L., De Filippis, L., Lecis, D., Vescovi, A. & Delia, D. DNA-damage response, survival and differentiation in vitro of a human neural stem cell line in relation to ATM expression. *Cell Death Differ.* **16**(6), 795–806. https://doi.org/10.1038/cdd.2009.10 (2009) (**Epub 2009/02/21**).
114. Yang, J. *et al.* The role of ROS and subsequent DNA-damage response in PUMA-induced apoptosis of ovarian cancer cells. *Oncotarget* **8**(14), 23492–23506. https://doi.org/10.18632/oncotarget.15626 (2017) (**Epub 2017/04/21**).
115. Nissanka, N. & Moraes, C. T. Mitochondrial DNA damage and reactive oxygen species in neurodegenerative disease. *FEBS Lett.* **592**(5), 728–742. https://doi.org/10.1002/1873-3468.12956 (2018) (**Epub 2017/12/28**).
116. Shi, T., van Soest, D. M. K., Polderman, P. E., Burgering, B. M. T. & Dansen, T. B. DNA damage and oxidant stress activate p53 through differential upstream signaling pathways. *Free Radic. Biol. Med.* https://doi.org/10.1016/j.freeradbiomed.2021.06.013 (2021) (**Epub 2021/06/19**).
117. Fischer, N. W., Prodeus, A., Malkin, D. & Gariépy, J. p53 oligomerization status modulates cell fate decisions between growth, arrest and apoptosis. *Cell Cycle* **15**(23), 3210–3219. https://doi.org/10.1080/15384101.2016.1241917 (2016) (**Epub 2016/10/19**).
118. Chehab, N. H., Malikzay, A., Stavridi, E. S. & Halazonetis, T. D. Phosphorylation of Ser-20 mediates stabilization of human p53 in response to DNA damage. *Proc. Natl. Acad. Sci. USA.* **96**(24), 13777–13782. https://doi.org/10.1073/pnas.96.24.13777 (1999) (**Epub 1999/11/26**).
119. Honda, R., Tanaka, H. & Yasuda, H. Oncoprotein MDM2 is a ubiquitin ligase E3 for tumor suppressor p53. *FEBS Lett.* **420**(1), 25–27. https://doi.org/10.1016/s0014-5793(97)01480-4 (1997) (**Epub 1998/02/05**).
120. Guo, Z., Kozlov, S., Lavin, M. F., Person, M. D. & Paull, T. T. ATM activation by oxidative stress. *Science* **330**(6003), 517–521. https://doi.org/10.1126/science.1192912 (2010) (**Epub 2010/10/23**).
121. Reed, S. M. & Quelle, D. E. p53 acetylation: Regulation and consequences. *Cancers* **7**(1), 30–69. https://doi.org/10.3390/cancers7010030 (2014) (**Epub 2014/12/30**).
122. Puca, R. *et al.* HIPK2 modulates p53 activity towards pro-apoptotic transcription. *Mol. Cancer.* **8**, 85. https://doi.org/10.1186/1476-4598-8-85 (2009) (**Epub 2009/10/16**).
123. Puca, R. *et al.* Nox1 is involved in p53 deacetylation and suppression of its transcriptional activity and apoptosis. *Free Radic. Biol. Med.* **48**(10), 1338–1346. https://doi.org/10.1016/j.freeradbiomed.2010.02.015 (2010) (**Epub 2010/02/23**).
124. Fogarty, M. P. *et al.* A role for p53 in the beta-amyloid-mediated regulation of the lysosomal system. *Neurobiol. Aging.* **31**(10), 1774–1786. https://doi.org/10.1016/j.neurobiolaging.2008.09.018 (2010) (**Epub 2008/12/09**).
125. Jung, E. S. *et al.* p53-dependent SIRT6 expression protects Aβ42-induced DNA damage. *Sci. Rep.* **6**, 25628. https://doi.org/10.1038/srep25628 (2016) (**Epub 2016/05/10**).
126. Lasagna-Reeves, C. A. *et al.* Dual role of p53 amyloid formation in cancer; loss of function and gain of toxicity. *Biochem. Biophys. Res. Commun.* **430**(3), 963–968. https://doi.org/10.1016/j.bbrc.2012.11.130 (2013) (**Epub 2012/12/25**).
127. Stanga, S., Lanni, C., Sinforiani, E., Mazzini, G. & Racchi, M. Searching for predictive blood biomarkers: Misfolded p53 in mild cognitive impairment. *Curr. Alzheimer Res.* **9**(10), 1191–1197. https://doi.org/10.2174/156720512804142886 (2012) (**Epub 2012/07/04**).
128. García, S. *et al.* Unfolded p53 as a marker of oxidative stress in mild cognitive impairment, Alzheimer's and Parkinson's disease. *Curr. Alzheimer Res.* **18**(9), 695–700. https://doi.org/10.2174/1567205018666211117101216 (2021) (**Epub 2021/11/19**).
129. Lanni, C., Uberti, D., Racchi, M., Govoni, S. & Memo, M. Unfolded p53: A potential biomarker for Alzheimer's disease. *J. Alzheimers Dis.* **12**(1), 93–99. https://doi.org/10.3233/jad-2007-12109 (2007) (**Epub 2007/09/14**).
130. Uberti, D. *et al.* Selective impairment of p53-mediated cell death in fibroblasts from sporadic Alzheimer's disease patients. *J. Cell Sci.* **115**(Pt 15), 3131–3138. https://doi.org/10.1242/jcs.115.15.3131 (2002) (**Epub 2002/07/16**).
131. Wang, G. & Fersht, A. R. Propagation of aggregated p53: Cross-reaction and coaggregation vs. seeding. *Proc. Natl. Acad. Sci. USA* **112**(8), 2443–2448. https://doi.org/10.1073/pnas.1500262112 (2015) (**Epub 2015/02/13**).
132. Ishimaru, D. *et al.* Cognate DNA stabilizes the tumor suppressor p53 and prevents misfolding and aggregation. *Biochemistry* **48**(26), 6126–6135. https://doi.org/10.1021/bi9003028 (2009) (**Epub 2009/06/10**).
133. Frain, L. *et al.* Association of cancer and Alzheimer's disease risk in a national cohort of veterans. *Alzheimer's Dementia* **13**(12), 1364–1370. https://doi.org/10.1016/j.jalz.2017.04.012 (2017) (**Epub 2017/07/18**).
134. Lee, J. E., Kim, D. & Lee, J. H. Association between Alzheimer's disease and cancer risk in South Korea: An 11-year Nationwide Population-Based Study. *Dement. Neurocogn. Disord.* **17**(4), 137–147. https://doi.org/10.12779/dnd.2018.17.4.137 (2018) (**Epub 2019/03/25**).
135. Zhang, D. D. *et al.* Investigating the association between cancer and dementia risk: A longitudinal cohort study. *Alzheimer's Res. Ther.* **14**(1), 146. https://doi.org/10.1186/s13195-022-01090-9 (2022) (**Epub 2022/10/06**).
136. Yu, X. *et al.* The STING phase-separator suppresses innate immune signalling. *Nat. Cell Biol.* **23**(4), 330–340. https://doi.org/10.1038/s41556-021-00659-0 (2021) (**Epub 2021/04/10**).
137. Yu, X., Zhao, Z. & Jiang, Z. Recent progress on the activation of the cGAS-STING pathway and its regulation by biomolecular condensation. *J. Mol. Cell Biol.* https://doi.org/10.1093/jmcb/mjac042 (2022) (**Epub 2022/07/09**).
138. Song, L. *et al.* Impaired type I interferon signaling activity implicated in the peripheral blood transcriptome of preclinical Alzheimer's disease. *EBioMedicine* **82**, 104175. https://doi.org/10.1016/j.ebiom.2022.104175 (2022) (**Epub 2022/07/22**).
139. Jin, M. *et al.* Type-I-interferon signaling drives microglial dysfunction and senescence in human iPSC models of Down syndrome and Alzheimer's disease. *Cell Stem Cell* **29**(7), 1135–53.e8. https://doi.org/10.1016/j.stem.2022.06.007 (2022) (**Epub 2022/07/09**).
140. Ueno, M. *et al.* Thioredoxin-dependent redox regulation of p53-mediated p21 activation. *J. Biol. Chem.* **274**(50), 35809–35815. https://doi.org/10.1074/jbc.274.50.35809 (1999) (**Epub 1999/12/10**).
141. Ravi, D., Muniyappa, H. & Das, K. C. Endogenous thioredoxin is required for redox cycling of anthracyclines and p53-dependent apoptosis in cancer cells. *J. Biol. Chem.* **280**(48), 40084–40096. https://doi.org/10.1074/jbc.M507192200 (2005) (**Epub 2005/09/15**).

142. Hanson, S., Kim, E. & Deppert, W. Redox factor 1 (Ref-1) enhances specific DNA binding of p53 by promoting p53 tetramerization. *Oncogene* **24**(9), 1641–1647. https://doi.org/10.1038/sj.onc.1208351 (2005) (**Epub 2005/01/28**).
143. Seemann, S. & Hainaut, P. Roles of thioredoxin reductase 1 and APE/Ref-1 in the control of basal p53 stability and activity. *Oncogene* **24**(24), 3853–3863. https://doi.org/10.1038/sj.onc.1208549 (2005) (**Epub 2005/04/13**).

Acknowledgements

We acknowledge the Human Brain and Spinal Fluid Resource Center, VA W Los Angeles Healthcare Center, Los Angeles, CA within the NIH funded NeuroBioBank for the provision of tissues. We appreciate the assistance of Komal Sodhi, M.D. with the ATM ELISA experiment.

Author contributions

T.J.N. conceived the project, designed the experiments, carried out experiments, analyzed the data, and wrote the manuscript. Y.X. carried out Western blots and HPLC experiments. All authors read and approved the final manuscript.

Competing interests

The authors declare no competing interests.

Additional information

Supplementary Information The online version contains supplementary material available at https://doi.org/10.1038/s41598-023-35533-6.

Correspondence and requests for materials should be addressed to T.J.N.

Reprints and permissions information is available at www.nature.com/reprints.

Publisher's note Springer Nature remains neutral with regard to jurisdictional claims in published maps and institutional affiliations.